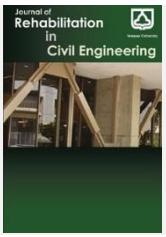

Journal of Rehabilitation in Civil Engineering

Journal homepage: https://civiljournal.semnan.ac.ir/

Impact Assessment of the Geometric Parameters of Steel Yielding Slit Damper on the Element Behavior

Ali Sadeghinia [1]; Mohammad Ali Kafi [2,*]; Majid Gholhaki [3]

1. Ph.D. Candidate, Faculty of Civil Engineering, Semnan University, Semnan, Iran
2. Associate Professor, Faculty of Civil Engineering, Semnan University, Semnan, Iran
3. Professor, Faculty of Civil Engineering, Semnan University, Semnan, Iran
* Corresponding author: *mkafi@semnan.ac.ir*

ARTICLE INFO

Article history:
Received: 05 December 2023
Revised: 23 June 2024
Accepted: 01 August 2024

Keywords:
Moment frame rehabilitation;
Steel slit damper;
Geometric impact assessment;
Cyclic loading;
Finite element analysis.

ABSTRACT

Concentric bracing systems are a popular solution for strengthening moment frames due to their high lateral stiffness, ease of installation, and low cost. However, buckling in compression members can result in sudden loss of strength and less deformability. Researchers have suggested using steel slit dampers to increase deformability and energy dissipation in this system by directing damage away from bracing members. In this study, 265 finite element models were analyzed in ABAQUS software based on previous experimental investigations and the installation configuration of the combined elliptical slit elements with Chevron bracing system in a moment frame. The effects of varying each geometric parameter of the element, including thickness, width, height, and number of slits, as well as the minor diameter of the elliptical slit, on the behavioral characteristics have been investigated in a three-dimensional parametric space. These characteristics are such as elastic stiffness, ductility, force capacity, and cyclic energy dissipation. Finally, and based on conducted numerical analysis, suitable ranges for each geometric parameter have been proposed to facilitate optimal design of the element.

E-ISSN: 2345-4423
© 2025 The Authors. Journal of Rehabilitation in Civil Engineering published by Semnan University Press.
This is an open access article under the CC-BY 4.0 license. (https://creativecommons.org/licenses/by/4.0/)

How to cite this article:
Sadeghinia, A., Kafi, M. A., & Gholhaki, M. (2025). Impact Assessment of the Geometric Parameters of Steel Yielding Slit Damper on the Element Behavior. Journal of Rehabilitation in Civil Engineering, (13)1, 96-112 .https://doi.org/10.22075/jrce.2024.32574.1949

1. Introduction

Over the years, the application of steel-yielding dampers has been widely proposed due to proper seismic performance and installation costs to strengthen structural frames. Moment connections, as well as concentric bracing systems, are the most frequently used in which these dampers have been applied. In a concentric bracing system, buckling in braces causes the structure to experience a sudden decline in stiffness and strength during seismic performance. In beam-to-column connections, similarly, stiffness and energy dissipation decrease during cyclic loading due to plastic area expansion from the beam to other elements of the moment connection. As mentioned previously, a suitable approach to improving the seismic behavior of a concentric bracing system is the application of yielding steel dampers such as ADAS and TADAS, proposed by Luis [1]. Furthermore, other types of yielding dampers that have been recently developed are steel-yielding elements with multiple slits. Conducted studies by Wada et al. revealed that steel-yielding elements with slits have a stable hysteresis curve [2]. After applying seismic displacement to the two ends of steel slit dampers (SSDs), the struts between the slits yield and become inelastic. Consequently, the absorbed seismic energy of the frame will be dissipated. The design and installation procedure of the SSDs must be in such a manner that the damper becomes inelastic before other frame elements; otherwise, the damper will act as an ordinary element without the ability to dissipate energy [3, 4]. Farahi and Mousavi [5] investigated the differences between the slit element with rectangular slits and with elliptical slits. Accordingly, their study revealed that the element with rectangular slits has considerable stress concentration at the two ends of each strut and cannot react entirely in a plastic manner. Conversely, the element with elliptical slits has a wide stress distribution and is capable of increasing seismic energy dissipation up to 99.6% in comparison to the element with rectangular slits. Lee et al. [6] proposed a new shape of slit that was similar to an hourglass to improve the performance of the rectangular slit damper. Experimental results under cyclic and monotonic loading showed a considerable increase in energy dissipation and strength. Moreover, they conducted a numerical and experimental study on the combination of a friction damper and a non-uniform slit element. Results indicated a rise in deformability and energy dissipation in the combined damper in comparison to the single one [7]. Ahmadie Amiri et al. [8] studied the behavior of a block slit element using finite element analysis and experimental models. Due to a lower length-to-thickness ratio in this element compared to others, shear capacity is higher, and the element is more economical. They found that reducing the element shape factor increases the shear capacity and energy dissipation of the element, but the displacement capacity will be reduced. Furthermore, increasing the element thickness will reduce the out-of-plane buckling of the sample. Finally, they discovered that the height-to-width ratio of the struts has a substantial impact on the overall behavior of the element, and by increasing this ratio, the area of hysteresis loops and energy dissipation of the element significantly rise. Saffari et al. [9] studied the impact of the slit element on the moment connections of the beam to the column in which the element was located at the top and bottom of the beam. They realized that the slit elements increase the absorption and dissipation of seismic energy at the connection area and reduce the plastic strength loss at the column flange. As a result, the geometry of the plastic hinge will almost be stable during cyclic loading, and the overall energy dissipation of the combined system will remarkably increase. Koken and Koroglu [10] conducted an experimental study on beam-to-column moment connections based on findings from welded connections in the Kobe and Northridge earthquakes. They developed a steel slit damper to reduce deformations in the beam and column. Zabihi-Samani [11] investigated the optimal configuration of the beam-to-column moment connection equipped with a slit element. They realized that the stiffness and damping of the element depend highly on the thickness, height, and number of slits. Liu et al. [12] studied six experimental samples of column connections and

column bases equipped with steel slit dampers and proposed a new configuration for this connection. Experimental evidence indicated that the column with the proposed connection had a remarkable performance in terms of stability, deformability, and lateral stiffness. It could be repaired in place for column drifts up to 3%. Moreover, the column could tolerate lateral loads up to the drift of 5%. Lee et al. [13] conducted a numerical and experimental study on the application of a steel slit damper in X-bracing systems to prevent buckling in braces. They found out that the slit element has stable hysteresis curves under shear forces and causes a considerable increase in the energy dissipation of the system. Chan and Albermani [14] experimentally investigated nine samples of a slit element with a thickness of 8 millimeters in a chevron bracing system. Considered variables in this study were the width and height of the slits, and results showed that the element with larger amounts of strut width and total length has higher deformability. On the contrary, they realized that the element with smaller strut width and total length has higher stiffness, so it will be damaged faster during cyclic loading. Kim and Jeong [15] studied the application effect of slit dampers in asymmetrical buildings. They proposed a method based on the level of seismic target performance and displacement response in the horizontal and vertical direction to determine the number and proper location of the dampers, aiming to reduce irregularities. Kim et al. [16] studied the retrofitting of existing buildings with steel slit dampers. They presented an algorithm for locating the dampers in buildings based on story drifts and capacity spectrum. NourEldin et al. [17] investigated the retrofitting of buildings with 3, 5, and 8 stories using a steel slit damper equipped with two shape memory alloy cables. After conducting nonlinear dynamic analysis and examining the fragility curves, the results indicated that due to the reversibility in the used cables, the behavior properties of the slit damper, especially the stiffness and energy dissipation capacity, were remarkably improved. Nik-hoosh and Kafi [18,19] conducted a numerical and experimental study on several steel slit dampers with different slit shapes. Firstly, he investigated 27 experimental samples with various slit shapes. Afterward, he conducted a finite element analysis on the models of experimental samples to precisely investigate each element with a different slit shape. The results implied that the elliptical shape of the slit element, considering the behavior properties including deformability, loading capacity, stiffness, and damage index, had the best performance among all. Finally, he presented an optimal shape for each element using optimization algorithms. Ahmadie Amiri et al. [20] conducted a numerical study on the effects of installing block slit dampers (BSDs) in a low-rise steel building with moment-resisting frames. Initially, they developed a simplified model of the damper based on experimental results and finite element analysis in Abaqus software. Subsequently, using the endurance time dynamic analysis method, they proposed a design procedure based on the performance of the aforementioned building and examined the results of installing the damper. The findings indicated that BSDs effectively reduced story drifts and absolute floor accelerations, suggesting their potential as an efficient system for retrofitting or designing moment-resisting frames. Kim et al. [21] conducted a study to investigate the effectiveness of a combined steel slit damper in controlling a structure's response to seismic loading. They presented two types of slit dampers in their research. The first model featured struts with varying geometrical specifications, while the second model had struts with different yield stresses. The study utilized both numerical simulations and experimental testing to analyze the performance of the two damper models. Oh and Park [22] investigated the impact of additional tensile forces on the cyclic behavior of a flexural yielding-type steel slit damper. The variables that were examined in their experimental model included shear loading and loading in a combination of shear and tension. The results showed that the cyclic behavior of the sample under shear loading was parallelogram-shaped, while under shear-tensile loading it was butterfly-shaped. Lee et al. [23] introduced a seismic control system with non-buckling slit dampers installed in a window configuration. They studied the impact of this system on a reinforced concrete moment frame. The findings revealed that the moment frame

without the control system experienced shear failure at a seismic intensity of 200 cm/s^2. On the other hand, the retrofitted moment frame with the proposed system and under the same loading experienced only minor damages. Rousta et al. [24] performed a finite element analysis on different types of metallic yielding dampers using pushover and cyclic analyses. The findings suggested that as the damper height increases, the effective stiffness and damping decrease. Moreover, Steel Plate Dampers (SPD) demonstrated the highest levels of stiffness and energy dissipation.

In the present study, mesh sensitivity analysis has been conducted on three models with different mesh sizes, and the results have been compared with the experimental ones from Nik-hoosh's study [18,19] to verify the finite element model in ABAQUS software [25]. After that, the effect of changing each geometrical parameter of the elliptical slit element on its behavior properties, including elastic stiffness, deformability, force capacity, and normalized hysteretic energy, has been thoroughly investigated. Finally, a suitable range for each geometrical parameter is proposed based on the aforementioned behavior properties of the element.

2. Basic model and loading protocol

The finite element model, based on Nik-hoosh's experimental sample [18,19], is presented in Fig. 1. To simulate the plastic behavior of steel material in ABAQUS, the Combined Hardening method with half-cycle data type is used based on the experimental findings of Nik-hoosh [18,19]. The experiment involved a tensile test conducted on a rectangular sample made of steel type ST37 and with dimensions of 8 mm by 10 mm and a length of 100 mm. The stress and strain values are represented in Fig. 2. The loading boundary conditions of the model are also presented in Fig. 1. Accordingly, the bottom flange of the element has all degrees of freedom fixed while only the degree of freedom in the direction of the cyclic load (Z direction) is free for the top flange. Therefore, similar to the lower flange, all other degrees of freedom in this flange are fixed. It is worth mentioning that the ABAQUS software can simulate out-of-plane buckling by considering the imperfection corresponding to the out-of-plane buckling modes of the element if necessary [25]

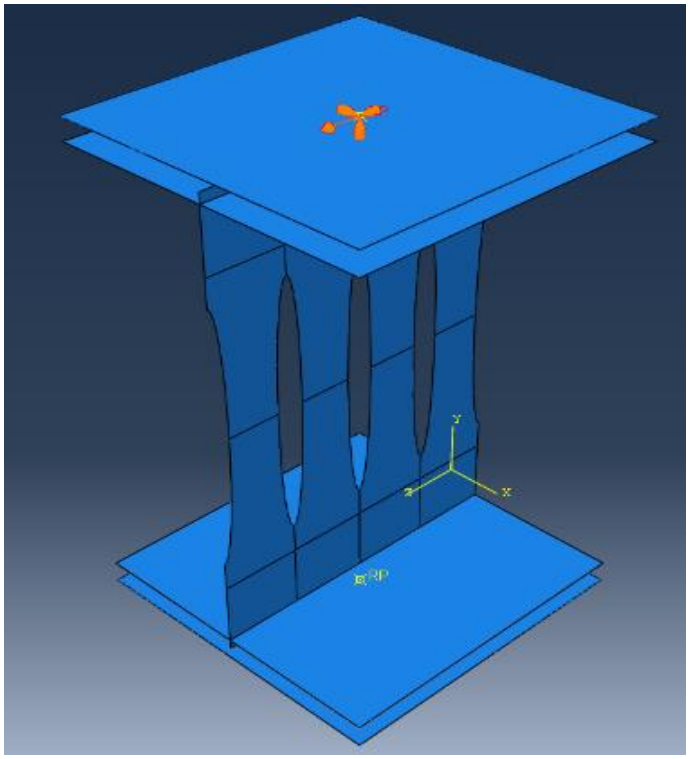

Fig. 1. The FEM model.

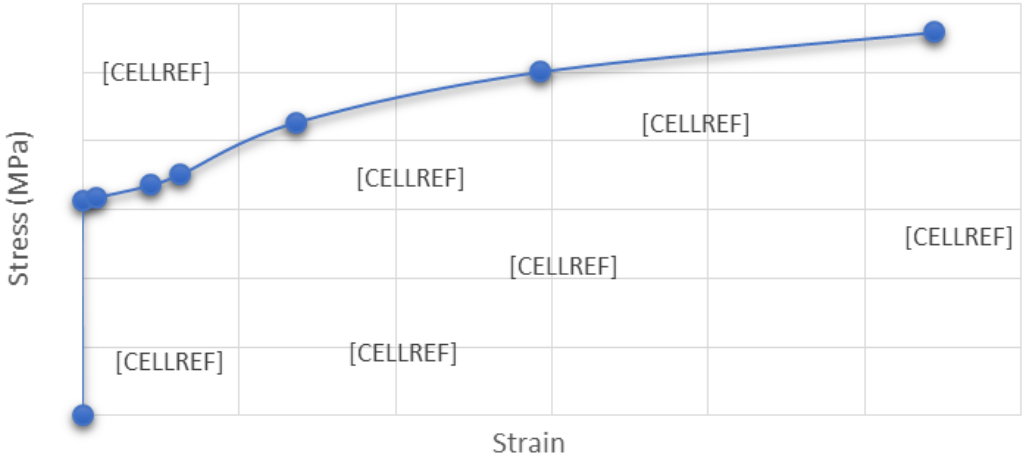

Fig. 2. Stress-strain values of the steel material in the model [18,19].

The dimensions of the FEM model are shown in Fig.3. All of them are in millimeters, and the web thickness is 8 millimeters.

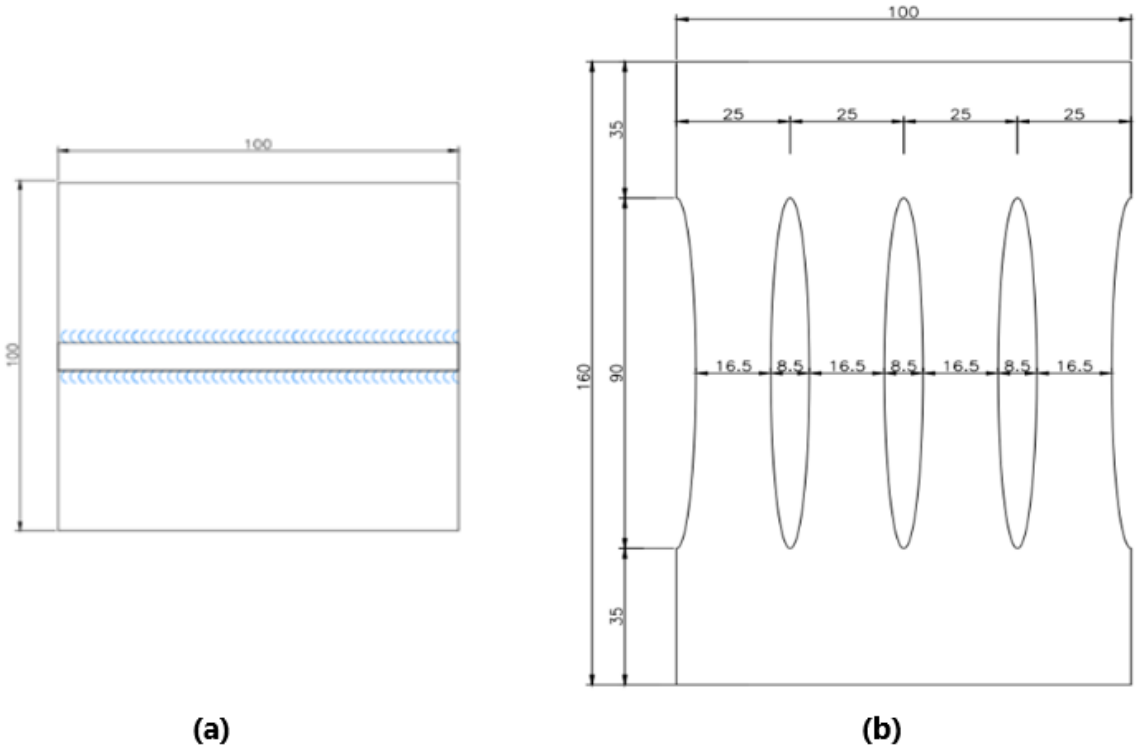

Fig. 3. Dimensions of the FEM model. (a) top view, (b) side view.

Additionally, the ductile damage model is used to simulate the progressive degradation of the steel material stiffness and strength due to plastic deformation in the finite element model. In ABAQUS, simulating ductile damage commonly involves using both damage initiation criteria and damage evolution laws. These elements work together to accurately define the progression of damage as a function of additional plastic deformation. The initiation of ductile damage is often defined using a ductile criterion based on fracture strain, stress triaxiality, and strain rate, and the evolution can be specified in terms of the equivalent plastic displacement or energy dissipation [25]. In this study, after performing calibration operations on the model, the parameters related to ductile damage in the software are defined in a tabular form for two conditions. In the first and second conditions,

respectively, the fracture strain is set to 1 and 0.5, the stress triaxiality is set to 0 and 0.4, and the strain rate for both conditions is set to 1. Additionally, the damage evolution is of the displacement type, and maximum degradation is considered, applied to the model as linear softening. The steel elastic modulus of the model is considered to be 218000 MPa based on the experimental sample [18,19]. The applied loading protocol, according to the experimental study, is based on the ATC 24 standard [26] and is presented in Fig. 4.

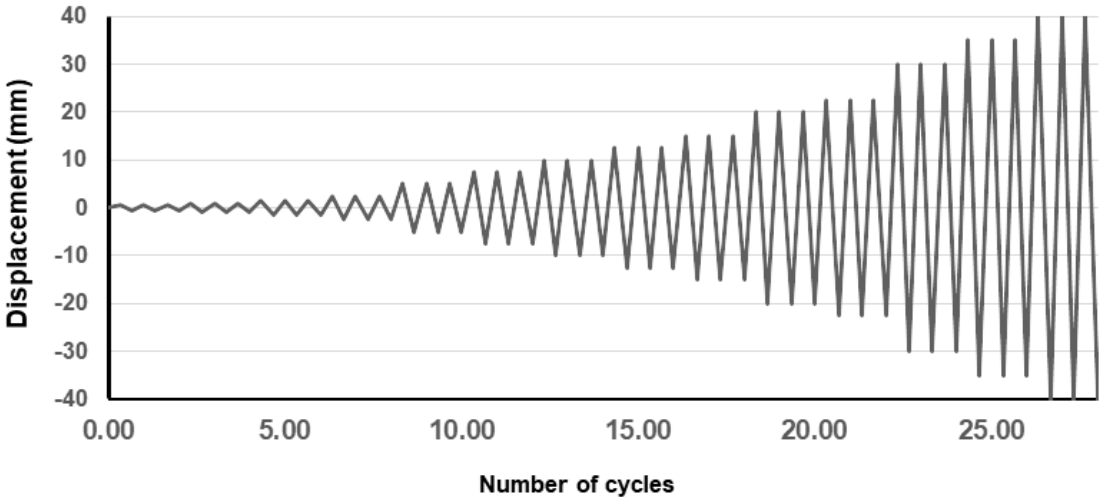

Fig. 4. Cyclic loading protocol [26].

The shell-homogeneous element is utilized to model the experimental sample in ABAQUS. After performing mesh sensitivity analysis on the model and comparing the resulting plots of the hysteresis loop and push of the hysteresis loop to those of the experimental sample, the approximate global size of the mesh in the model is chosen to be 3 millimeters. The related plots are demonstrated in Fig. 5.

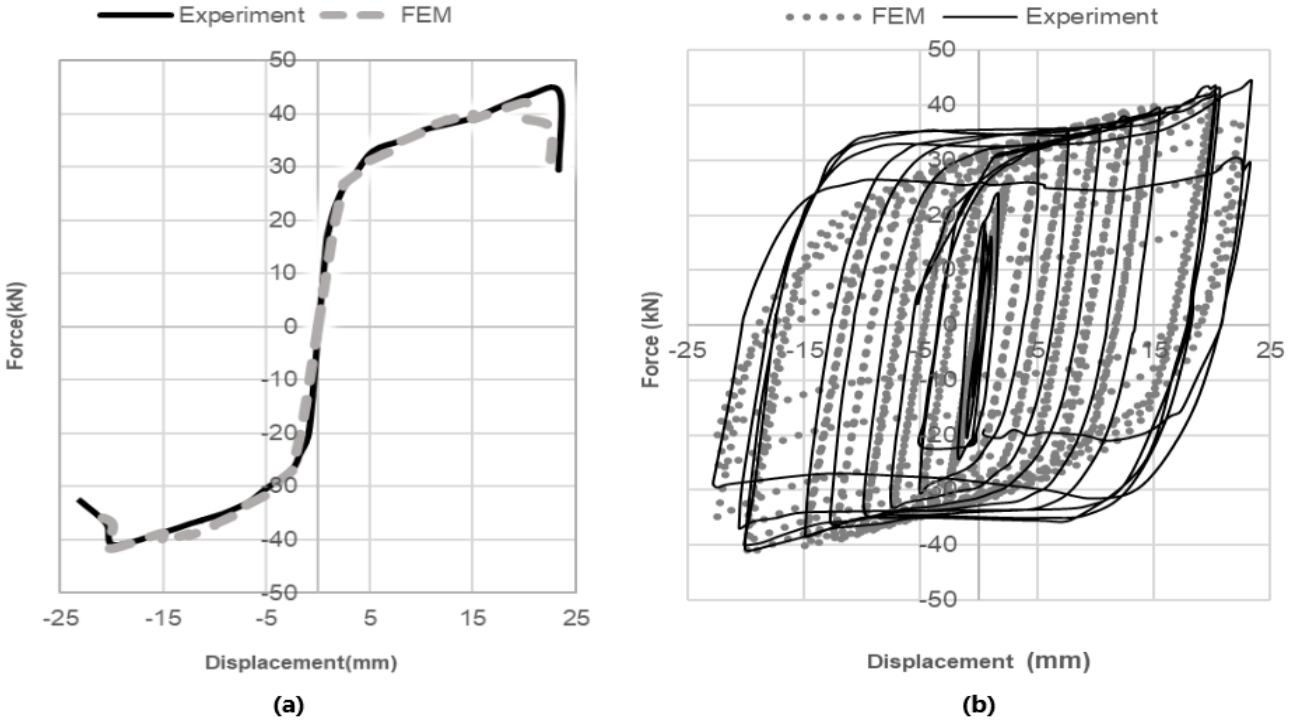

Fig. 5. Comparison of hysteresis loop and envelope curve of experimental sample [18,19] and FEM model. (a) envelope curves, (b) hysteresis loops.

Finally, for a more accurate comparison of the defined damage model in the software with the experimental sample [18,19], the stress distribution of the finite element model is presented in Fig.6(a) and the corresponding experimental sample is shown in Fig. 6(b).

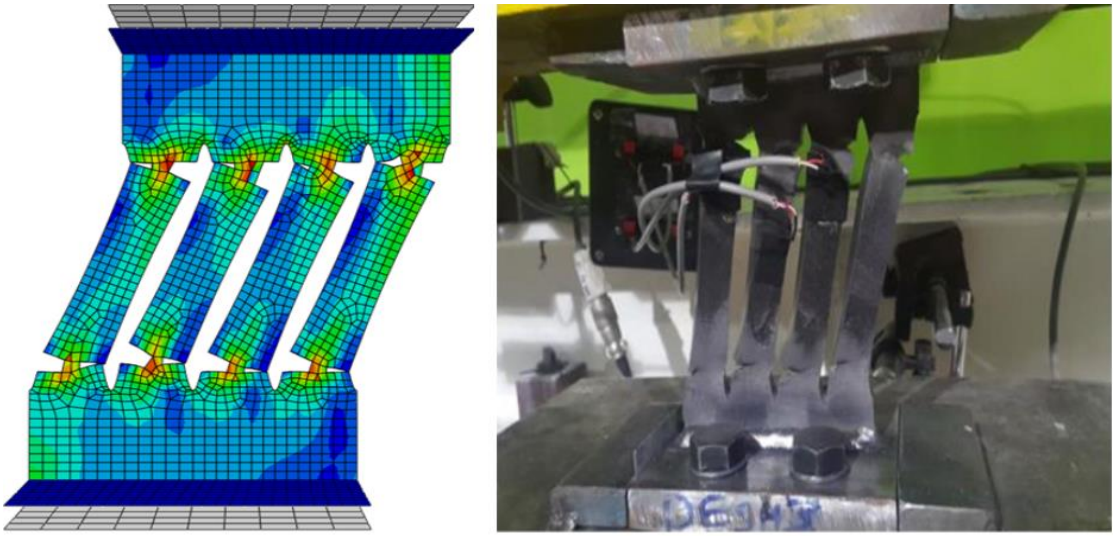

(a) (b)

Fig. 6. Comparison of damage distribution. (a) FE model, (b) experimental sample [18,19].

3. Parametric models and element behavior

The geometrical parameters investigated in this study are the height-to-width ratio of the strut (h/b), the ratio of space between the slits and flange to the strut height (h'/h), the proportion of the minor diameter of the slit to the strut height (d/h), the ratio of thickness to strut width (t/b), and the number of slits (n). All these parameters are shown in Fig. 7.

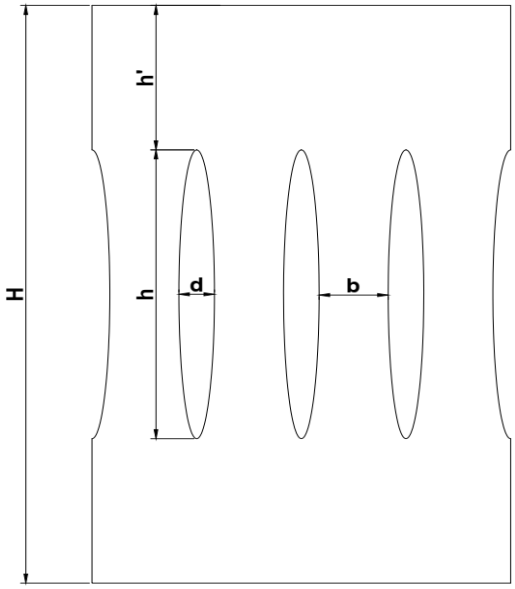

Fig. 7. Geometrical parameters.

Based on the performed research projects about the slit dampers and the method of installation in the frame presented in Fig. 8, each strut between the slits acts as a beam with fixed supports at both ends, in which the strut height and the strut width represent the beam span and the beam profile height, respectively. Moreover, the Timoshenko beam theory [27] has been considered to produce

and survey several finite element models with different geometrical parameters. According to this theory and the results of other studies, the flexural or shear behavior in a beam depends highly on the ratio of length to thickness. If the ratio becomes greater than 10, the deformations in the beam are mainly due to bending rather than shear, and vice versa [28-30]. Consequently, the ratio of height to width of the strut (h/b) has a major effect on behavior properties based on the yielding mechanism of the element, and the effects of this parameter have been investigated at the first stage. Several finite element models have been produced to observe the effect of (h/b) on element behavior, and only the (h/b) ratio is different between the models. Other geometrical parameters are considered to be constant in this stage.

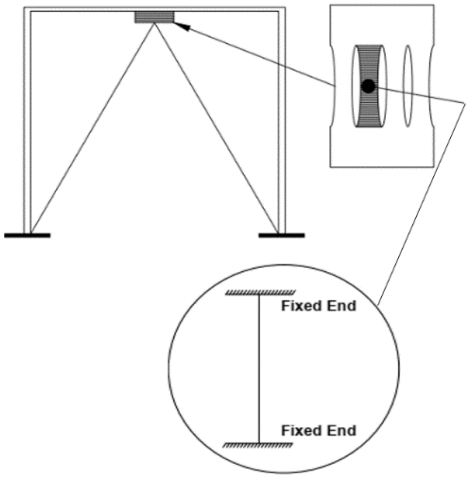

Fig. 8. Method of installation in moment frame.

4. Element behavioral properties

To study the effects of each geometrical property of the element, four seismic behavior properties, including deformability (μ), force capacity, elastic stiffness (Ke), and normalized hysteretic energy (E_{D_N}), have been considered and calculated based on the following. After producing the plots of the hysteresis push loop based on the obtained results from the ABAQUS models, each plot has been transformed into a bilinear plot according to the EEEP method of ASTM E2126 standard [31] to calculate the behavior properties. Then, by utilizing the bilinear plot and related equations from the standard, elastic stiffness, yield load (Py), ultimate displacement (Du), and yield displacement (Dy) for each model are calculated. Finally, equations (1) to (4) determine the behavior properties for each model.

$$\mu = \frac{D_u}{D_y} \tag{1}$$

$$P_y = \left(D_u - \sqrt{D_u{}^2 - \frac{2A}{K_e}} \right) \times K_e \tag{2}$$

$$K_e = \frac{0.4P_{max}}{D_e} \tag{3}$$

$$\text{Ideal\_Force\_Index} = \frac{P_{max}}{P_y} \tag{4}$$

It is crucial to mention that enlarging the dimensions of each model increases the maximum possible displacement and maximum bearable load. Consequently, hysteretic energy in models with larger dimensions is much greater than in smaller models. Therefore, this behavior property is not suitable for comparing the models with each other. In this regard, the hysteresis loops in each model are normalized to their maximum applied force and Du at first. Then the hysteretic energy is calculated from the normalized plot. In the above equations, Pmax, Ke, De, and A represent the maximum applied force, elastic stiffness, the displacement related to 40% of Pmax, and the area under the envelope curve until Du, respectively.

5. Effects of h/b

As mentioned earlier, the h/b ratio has a significant role in the overall mechanism of the slit element. Accordingly, to investigate the effect of altering this ratio, various models are produced in a way that the value of h remains constant and equal to that of the basic model shown in Fig. 3, while the value of b is variable. Given that the b value is variable in these models, the t/b ratio would also change simultaneously. To prevent this, the thickness (t) in these models was selected in such a way that the t/b ratio remains constant and equal to that of the basic model (0.5), despite changes in b. It should be noted that other geometric parameters, including h'/h and d/h, remain unchanged and equal to those of the basic model, as the h value is assumed to be constant in this section. Increments in the range of 1 to 10 are considered to be 0.25. According to the results of other research about flexural and shear behavior in Timoshenko beam theory [27-30], and aiming to minimize the number of required models as possible, the increments for the h/b ratios more than 10 are considered to be 0.5. According to the diagrams presented in Fig. 9, it can be observed that by increasing the h/b ratio, the mentioned behavior properties generally increase continuously, and in the range of 8 to 10, each characteristic reaches its maximum.

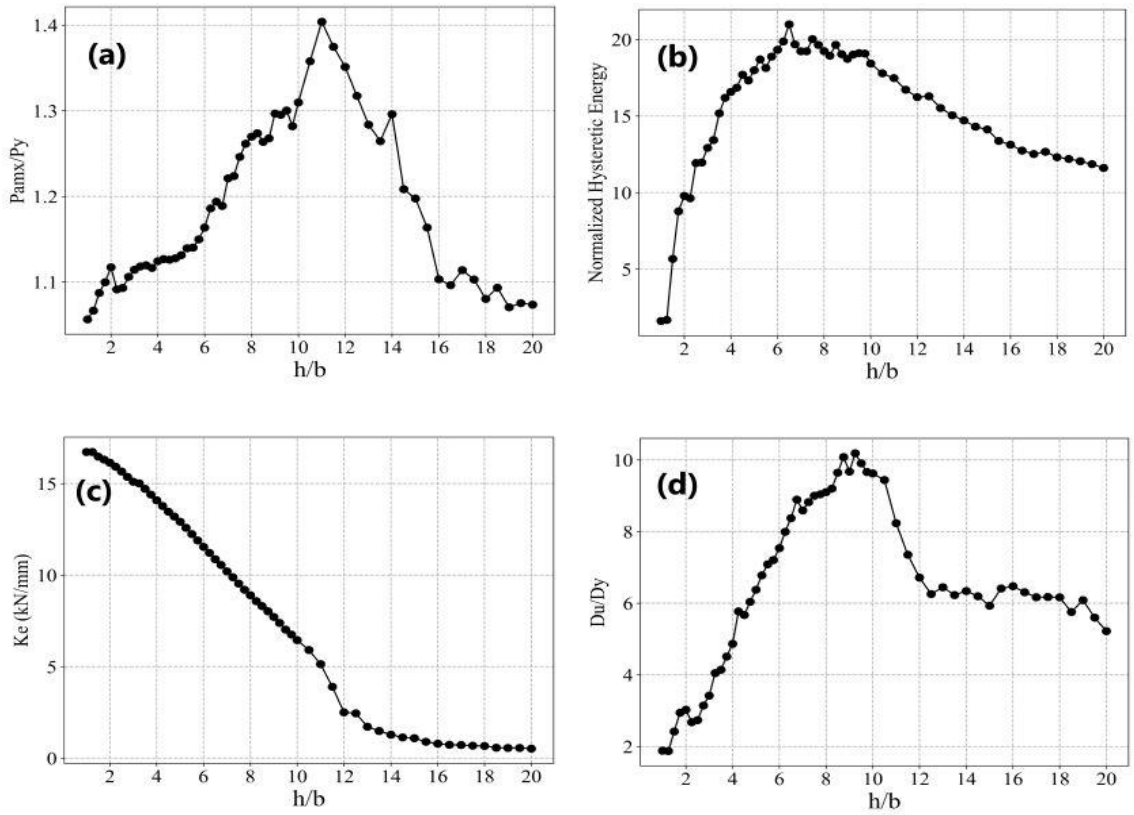

Fig. 9. Effects of increasing h/b on (a) ideal force index, (b) hysteretic energy, (c) elastic stiffness, (d) deformability.

However, for values of h/b greater than 10 and with the dominance of flexural behavior, the level of fragility increases, and generally, the energy dissipation capacity and stiffness in the element decrease significantly. According to the ideal force index diagram, the force capacity from h/b equal to 15.5 onwards will reach its minimum value. For better clarification of the element's behavior, it is important to note that the force index is influenced by both the element's deformability and elastic stiffness, which are defined in the ASTM E2126 [31] standard. By examining the force index diagram and equation (2), it is obvious that as the h/b ratio increases, the value of Pmax also increases. However, due to the decreasing slope of the Ke value compared to the increasing slope of the deformability diagram, the value of Py decreases. This leads to a significant increase with a steep slope up to an approximate h/b ratio of 10. As the h/b ratio continues to increase, the element's ability to withstand force in the plastic zone decreases, resulting in a decrease in the Pmax. This is due to the increasing dominance of flexural behavior and the decrease in deformability. Therefore, for considering optimal behavior for all behavioral properties of the slit element, the range of 3 to 8 is suitable. As a result, this range has been chosen as the optimal range for h/b ratios.

After examining the geometric parameter of h/b and determining the optimal range, models have been generated in a three-dimensional parametric space, as shown in Fig. 10, to investigate the effect of changing other mentioned geometric parameters. In this space, the h/b ratio and each of the geometric parameters, including h'/h, t/b, and d/h, are independent variables, while each of the behavior properties of the element is a dependent variable. To assess the effect of changing the number of slits, other geometric parameters are held constant, and only the number of slits varies. The values for each of these parameters for each model are presented in Table 1.

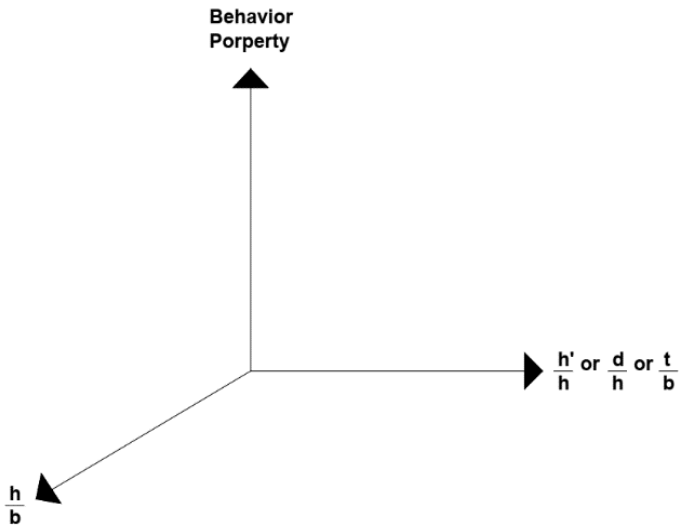

Fig. 10. 3D parametric space of analysis.

Table 1. Shape parameter range and step.

Shape Parameter	Range	Step
h/b	3-8	1
h'/h	0.1-1.4	0.1
d/h	0.1-1	0.1
t/b	0.1-1	0.1

6. Effects of h'/h

With regard to the geometry of the slit element, the space between the slits up to each of the flanges has a significant impact on the deformability, stiffness, and energy dissipation of the element.

Hence, the effect of variations in this space has been investigated. In this regard, various models have been generated within the range of h/b variations from 3 to 8, where h is constant, h' is variable, and other geometric parameters are considered to be constant and equal to those of basic model shown in Fig.3. The h'/h ratio varies in the range of 0.1 to 1.4 with increments of 0.1. The effect of variations in h'/h on each of the behavior properties is presented in Fig. 11.

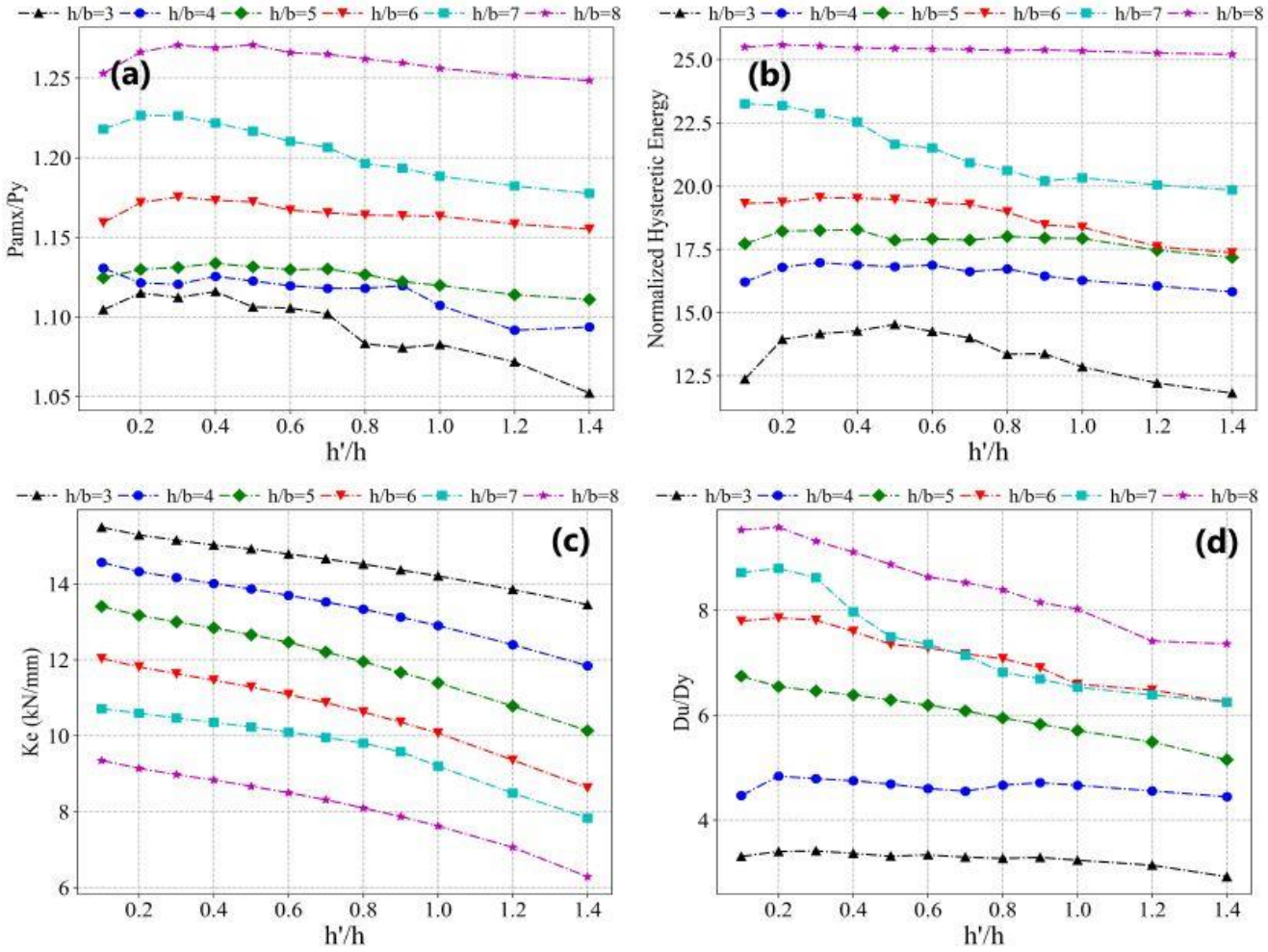

Fig. 11. Effects of increasing h'/h on (a) ideal force index, (b) hysteretic energy, (c) elastic stiffness, (d) deformability.

According to this figure and for almost all h/b ratios, hysteretic energy generally increases with a gentle slope when h'/h ratio rises from 0.2 to 0.8 and then decreases. In other words, in models with smaller h/b ratios, given the greater predominance of shear behavior compared to models with larger h/b ratios, increasing h'/h has a more significant effect on enhancing the energy dissipation capacity of the specimen. This is because in these models, with the shear behavior approximately constant, a larger volume of materials participates in energy dissipation and plastic behavior. However, with an excessive increase in the h'/h ratio, the flexural behavior abruptly affects the element, leading to a decrease in deformability and energy dissipation. The ideal force index increases normally with a rise in the h'/h ratio, but it undergoes a reduction after reaching a value of 0.6. Changes in h'/h have a more pronounced effect on the variation of the ideal force index at smaller h/b ratios. Deformability generally increases with a rise in the h'/h ratio up to a value of 0.3, but after that, it decreases. This reduction becomes more pronounced with higher h/b ratios. Finally, the elastic stiffness in the slit element generally decreases with an increase in the h'/h ratio. However, the slope of this reduction on the curve becomes steeper when the h/b ratio increases in

the element. As a result, the appropriate range for the h'/h ratio, where all behavior properties of the slit element collectively exhibit their maximum values, is between 0.2 and 0.4.

7. Effects of t/b

As previously mentioned, different thickness values (t) significantly impact the seismic behavior properties of the element. Various models have been generated to investigate the effect of thickness variations within the range of h/b ratios from 3 to 8. In these models, b is constant, t is variable, and the t/b ratio varies in the range of 0.1 to 1 with increments of 0.1. It is important to note that other geometric parameters are constant and equal to those of the basic model. The effect of t/b variations on each of the behavior properties is presented in Fig. 12.

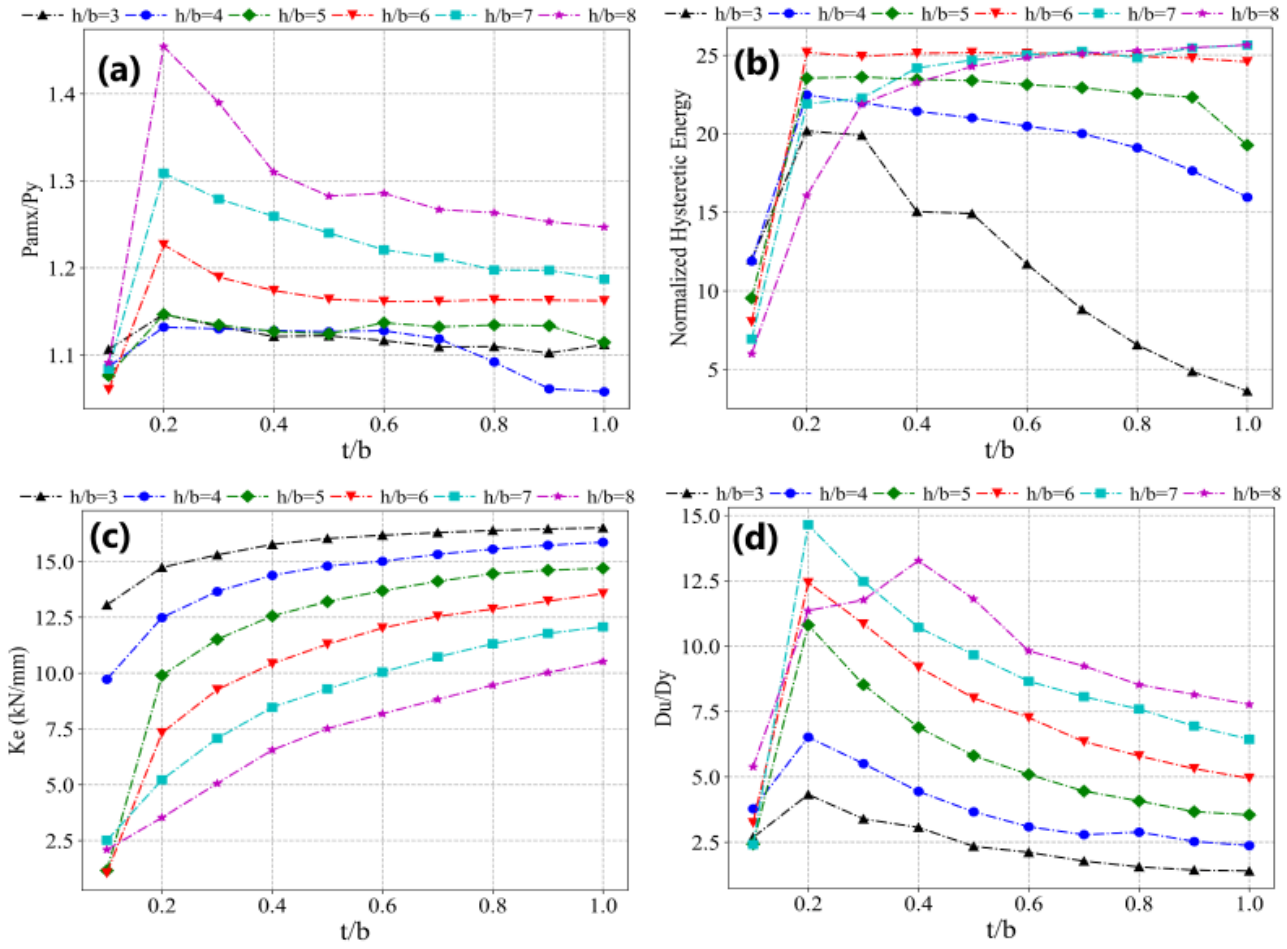

Fig. 12. Effects of increasing t/b on (a) ideal force index, (b) hysteretic energy, (c) elastic stiffness, (d) deformability.

It can be observed that hysteretic energy increases with a rise in the t/b ratio up to a value of 0.3 in models with a h/b smaller than 6 and up to a value of 0.7 in other models. Also, this behavior property in models with h/b greater than 6, despite the increasing dominance of flexural behavior, do not normally exhibit a tendency to reduce by increasing the t/b ratio. The ideal force index decreases by increasing the t/b ratio from a value of 0.2 onwards. However, this rate of reduction becomes steeper by increasing the h/b ratio. The deformability values in the element generally behave similarly to the ideal force index in a way that decreases by increasing the t/b ratio from a value of 0.2 onwards. However, this behavior is different in the model with a h/b value of 8, where the deformability increases up to a t/b ratio of 0.4. The reason for these conditions, considering the

corresponding plots of elastic stiffness and deformability, is the increase in the volume of energy-dissipating materials and consequently the enlargement of hysteresis loops in the initial cycles of the plastic region. It is noteworthy that, according to the elastic stiffness plot, increasing t/b leads to an increase in Dy, while the value of Du undergoes relatively minor changes. Consequently, deformability gradually decreases with the increase in the t/b ratio. Elastic stiffness in the slit element also generally decreases with an increase in the t/b ratio to values greater than 0.2. Finally, as observed in Fig. 12, the elastic stiffness generally increases with an increase in the t/b ratio. However, its effect is significantly more pronounced on models with a h/b greater than 4. Furthermore, increasing the t/b ratio up to 0.5 in models with a h/b ranging from 5 to 7 leads to a steeper increase in elastic stiffness compared to other models.

8. Effects of d/h

Various models have been generated in such a method that the h/b ratio varies from 3 to 8 to examine the effect of variations in the small to large diameter d/h ratio of the elliptical slit. In these models, h is constant, d is variable, and the d/h ratio varies in the range of 0.1 to 1 with increments of 0.1. Other geometric parameters are kept constant and equal to those of the basic model shown in Fig. 3. The effect of d/h variations on each of the behavior properties is presented in Fig. 13.

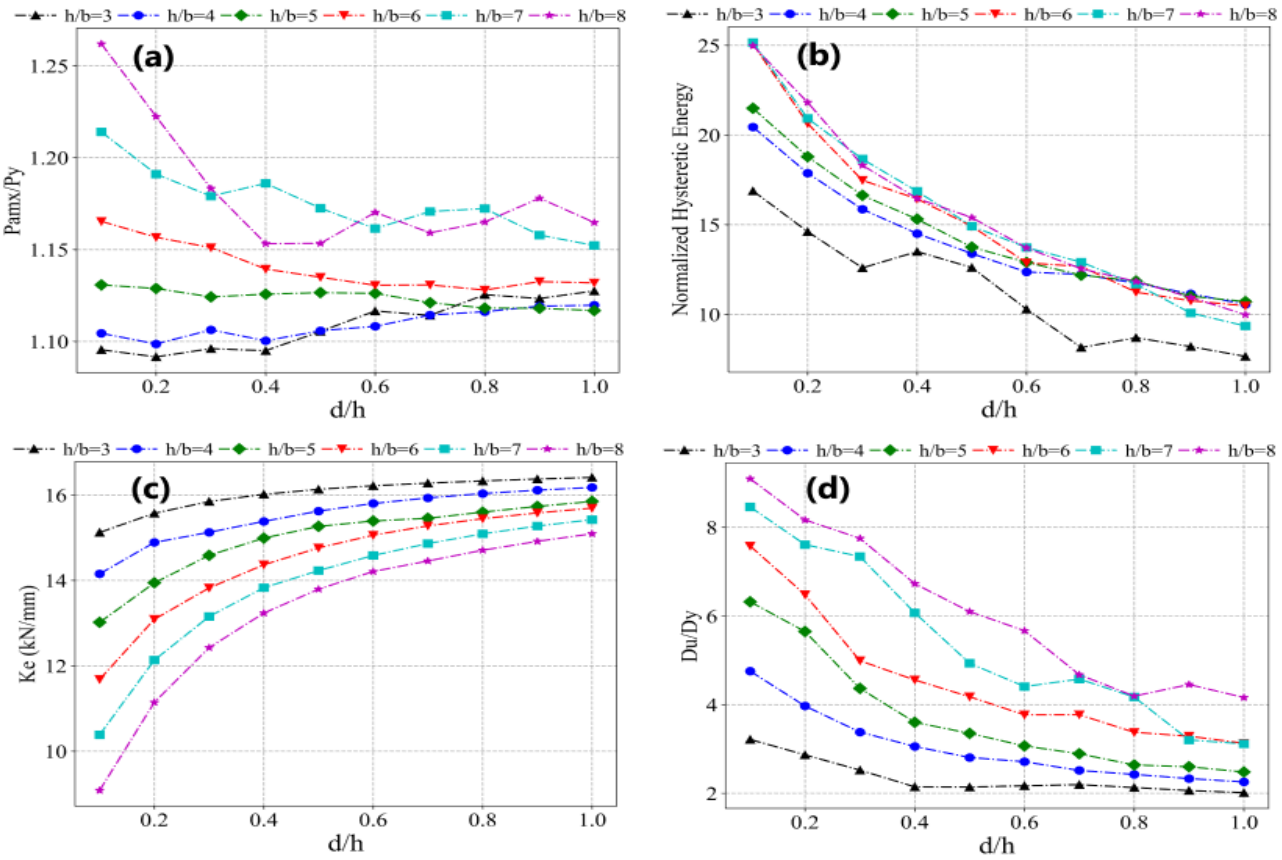

Fig. 13. Effects of increasing d/h on (a) ideal force index, (b) hysteretic energy, (c) elastic stiffness, (d) deformability.

According to this figure, it is observed that with an increase in the d/h ratio in all h/b ratios under consideration, hysteretic energy generally decreases, and the slope of the curve is slower in models with smaller h/b ratios. Moreover, in almost all h/b ratios in process, with an increase in d/h ratio to a value greater than 0.4, the slope of the curve becomes steeper. The ideal force index does not exhibit a consistent behavior while increasing the d/h ratio in models with different h/b proportions.

In models with h/b ratios less than 5, due to the greater dominance of shear behavior over flexural behavior, an increase in d/h to values greater than 0.5 results in a slight increase in the ideal force index. However, in models with h/b ratios greater than 5, increasing the h/b ratio results in the growth of flexural behavior, and increasing the ratio of small to large diameter of the elliptical slit up to the value of 0.4 leads to a decrease in this index. For the ratios Beyond 0.4, the slope of the curve becomes gentler. The deformability of the slit element decreases when the d/h ratio increases in all models, and the slope of the curve is steeper in models with greater h/b. Elastic stiffness increases with a rise in the diameter ratio for all h/b values. However, in models with a larger h/b ratio, given the greater dominance of flexural behavior, this property shows higher sensitivity to changes in d/h. Ultimately, beyond a d/h ratio of 0.6, changes in elastic stiffness continue with a relatively low slope across all h/b ratios.

9. Effects of number of slits (n)

To investigate the effect of changes in the number of slits (n), various models based on the geometric properties of the base model presented in Fig. 3 have been examined. In these models, only the number of slits varies from 3 to 9, while other geometric parameters remain constant. The effect of changes in the number of slits on the behavior properties of the element is presented in Fig. 14.

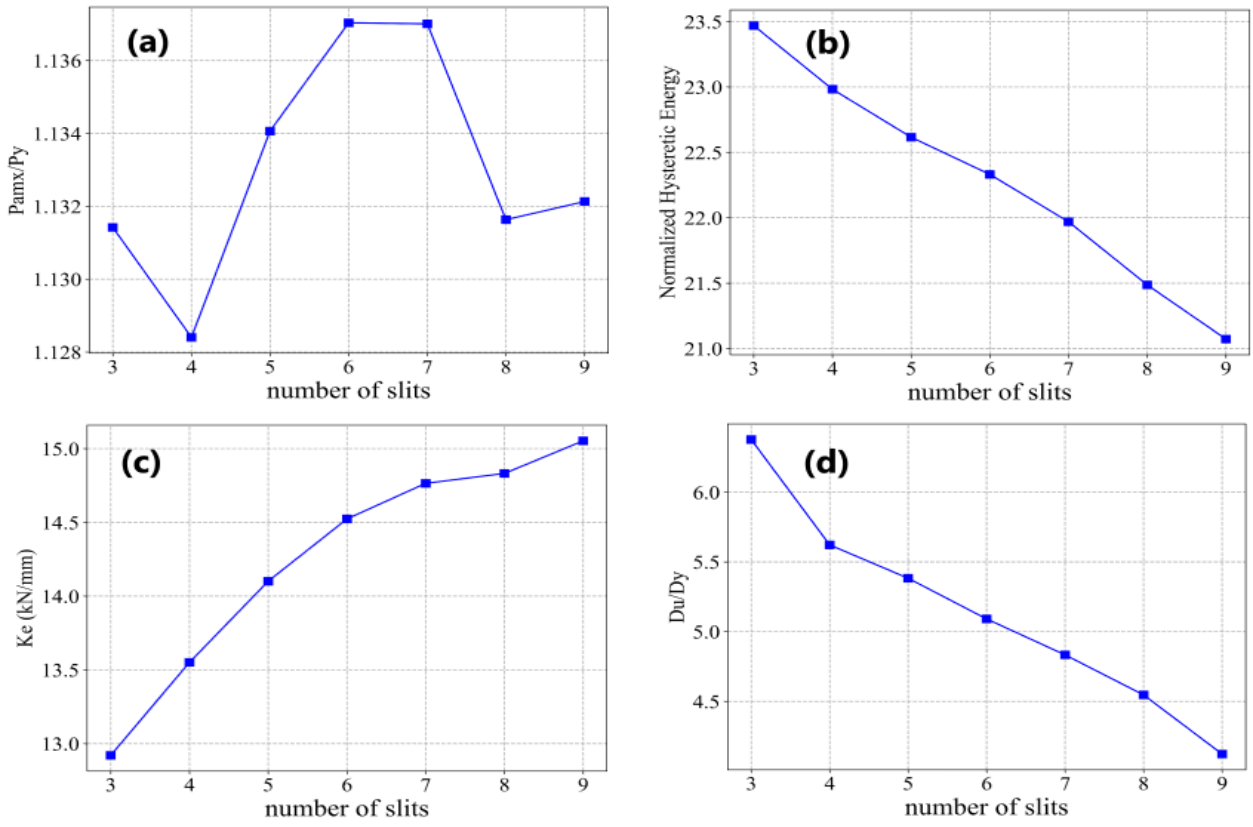

Fig. 14. Effects of increasing number of slits on (a) ideal force index, (b) hysteretic energy, (c) elastic stiffness, (d) deformability.

Based on this figure, it is observed that with an increase in the number of slits, hysteretic energy and deformability in the element decrease, and the ideal force index and elastic stiffness increase. However, the extent of these changes is not significant compared to the increase in the number of slits. With a threefold increase in the number of slits from the initial value, the normalized hysteretic energy and deformability decrease by 10% and 35%, respectively, and the elastic stiffness increases

by 15%. The ideal force index remains almost unchanged with an increase in the number of slits, and according to the corresponding graph, it changes by a maximum of 1% at its highest value compared to the initial value. Moreover, to further investigate the reason for the element's behavior in this section, the stress distribution in the element has been examined in two scenarios: one with 4 slots and the other with 9 slots, as depicted in Fig. 15. Accordingly, it is observed that the stress distribution in the element with 4 slits is much more extensive compared to the configuration with 9 slits. In the element with 9 slits, the majority of stresses are concentrated at the ends of the struts. Furthermore, it is evident that in the element with 4 slits, some of the space between the slits and flanges of the element contributes to stress resistance, whereas in the element with 9 slits, the level of stress generated in this space is minimal. It is worth mentioning that the topic discussed has been briefly investigated by Nik-hoosh's experimental research [18,19], where it was stated that increasing the length of the element by more than approximately 25% of its height (with other geometric parameters held constant) negatively affects its behavioral characteristics and gradually increases the likelihood of sudden failure in the element.

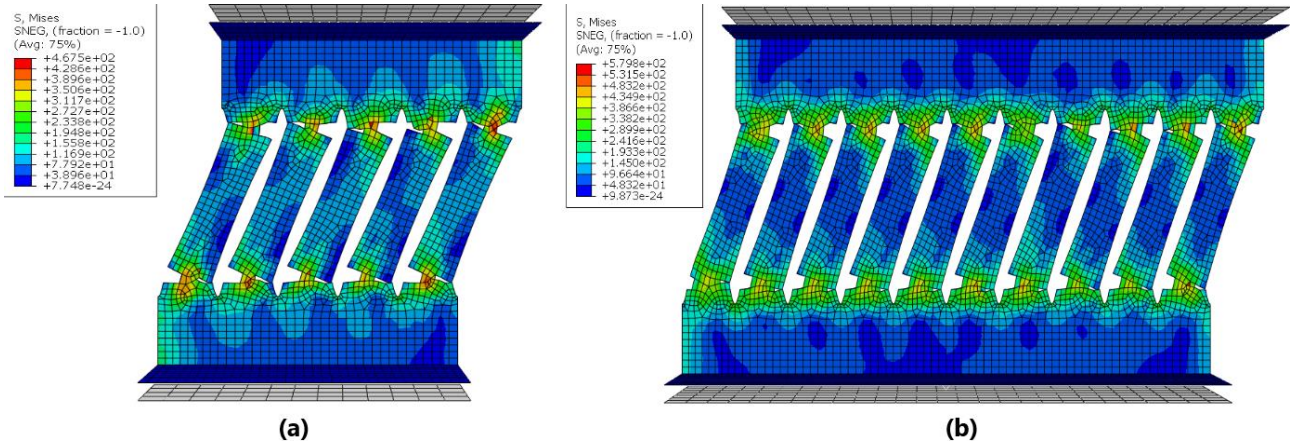

Fig. 15. Stress distribution in elements with (a) 4-slits and (b) 9-slits.

10. Conclusion

In this study, a comprehensive evaluation of the effects of variations in each geometric parameter constituting the elliptical slit element was conducted using finite element analysis with 265 ABAQUS software models. The behavior of this element, based on previous research results, resembles that of a Timoshenko beam with fixed supports, and consequently, the aspect ratio (length-to-thickness ratio in the beam) significantly influences both flexural and shear behavior. In this regard, initially, the aspect ratio of height to strut width (h/b) in the element, equivalent to the aspect ratio of length to thickness in the Timoshenko beam, was examined. It was observed that the slit element exhibits favorable behavior within the range of 3 to 8 for this ratio. Subsequently, considering the substantial impact of aspect ratio on seismic behavior properties, other geometric parameters were investigated for each h/b ratio within the mentioned range. Furthermore, based on the obtained results, the influence of each geometric parameter on behavior properties is discernible, with the aspect ratio and t/b having the most significant effects on the element's behavior. Moreover, it should be noted that increasing the number of slots has not significantly affected the behavioral characteristics of the damper, but intuitively, it leads to an increase in the elastic stiffness of the damper proportional to the number of added slots. However, exceeding this variable to an extent that significantly increases the aspect ratio of the damper's length to its height can adversely affect its ductility and energy dissipation capacity. Finally, to make the design process of this element faster and easier while ensuring optimal performance, Table 2 provides the proposed

appropriate range and examination results of the influence of each geometric parameter on behavior properties.

Table 2. Appropriate range for geometrical parameters.

Parameter	$\frac{h}{b}$	$\frac{h'}{h}$	$\frac{t}{b}$	$\frac{d}{h}$
Suitable Range	3 - 8	0.2 - 0.4	0.2 – 0.5	0.1 -0.4

Funding

This research did not receive any specific grant from funding agencies in the public, commercial, or not-for-profit sectors.

Conflicts of interest

The authors declare that they have no known competing financial interests or personal relationships that could have appeared to influence the work reported in this paper.

Authors contribution statement

Ali Sadeghinia: Conceptualization, Investigation, Methodology, Software, Formal analysis, Writing - original draft.

Mohammad Ali Kafi: Supervision, Conceptualization, Methodology, Writing - review & editing.

Majid Gholhaki: Supervision, Methodology, Writing - review & editing.:

References

[1] Luis M. Seismic Design of Energy Dissipation Systems for Optimal Structural Performance Optimal Structural Performance. PhD Virginia Polytech Inst State Univ 2000.

[2] Wada A, Huang YH, Yamada T, Ono Y, Sugiyama S, Baba M, et al. Actual size and real time speed tests for hysteretic steel damper. Proc STESSA 1997;97:778–85.

[3] Oh SH, Kim YJ, Ryu HS. Seismic performance of steel structures with slit dampers. Eng Struct 2009;31. https://doi.org/10.1016/j.engstruct.2009.03.003.

[4] Benavent-Climent A. A brace-type seismic damper based on yielding the walls of hollow structural sections. Eng Struct 2010;32. https://doi.org/10.1016/j.engstruct.2009.12.037.

[5] Farahi Shahri S, Mousavi SR. Application of Elliptic Slits for Development of Slit Damper in Beam-to-Column Connection. Modares Civ Eng J 2016;16:93–102.

[6] Lee CH, Lho SH, Kim DH, Oh J, Ju YK. Hourglass-shaped strip damper subjected to monotonic and cyclic loadings. Eng Struct 2016;119. https://doi.org/10.1016/j.engstruct.2016.04.019.

[7] Lee CH, Kim J, Kim DH, Ryu J, Ju YK. Numerical and experimental analysis of combined behavior of shear-type friction damper and non-uniform strip damper for multi-level seismic protection. Eng Struct 2016;114. https://doi.org/10.1016/j.engstruct.2016.02.007.

[8] Ahmadie Amiri H, Najafabadi EP, Estekanchi HE. Experimental and analytical study of Block Slit Damper. J Constr Steel Res 2018;141. https://doi.org/10.1016/j.jcsr.2017.11.006.

[9] Saffari H, Hedayat AA, Nejad MP. Post-Northridge connections with slit dampers to enhance strength and ductility. J Constr Steel Res 2013;80. https://doi.org/10.1016/j.jcsr.2012.09.023.

[10] Köken A, Köroğlu MA. Experimental Study on Beam-to-Column Connections of Steel Frame Structures with Steel Slit Dampers. J Perform Constr Facil 2015;29. https://doi.org/10.1061/(asce)cf.1943-5509.0000553.

[11] Zabihi-Samani M. Design of Optimal Slit Steel Damper Under Cyclic Loading for Special Moment Frame by Cuckoo Search. Int J Steel Struct 2019;19. https://doi.org/10.1007/s13296-019-00206-6.

[12] Liu Y, Guo Z, Liu X, Chicchi R, Shahrooz B. An innovative resilient rocking column with replaceable steel slit dampers: Experimental program on seismic performance. Eng Struct 2019;183. https://doi.org/10.1016/j.engstruct.2019.01.059.

[13] Lee MH, Huh C, Yoon MH. Ultimate energy absorption capacity of steel plate slit dampers subjected to shear force. Int J Steel Struct 2002;2:71–9.

[14] Chan RWK, Albermani F. Experimental study of steel slit damper for passive energy dissipation. Eng Struct 2008;30. https://doi.org/10.1016/j.engstruct.2007.07.005.

[15] Kim J, Jeong J. Seismic retrofit of asymmetric structures using steel plate slit dampers. J Constr Steel Res 2016;120. https://doi.org/10.1016/j.jcsr.2016.02.001.

[16] Kim J, Kim M, Eldin MN. Optimal distribution of steel plate slit dampers for seismic retrofit of structures. Steel Compos Struct 2017;25. https://doi.org/10.12989/scs.2017.25.4.473.

[17] NourEldin M, Naeem A, Kim J. Life-cycle cost evaluation of steel structures retrofitted with steel slit damper and shape memory alloy–based hybrid damper. Adv Struct Eng 2019;22. https://doi.org/10.1177/1369433218773487.

[18] Nik-hoosh K. Introduction of modified Steel Slit Dampers, based on experimental and numerical studies under cyclic loading. Semnan University, 2019.

[19] Kafi MA, Nik-Hoosh K. The geometric shape effect of steel slit dampers in their behavior. Mag Civ Eng 2019;87. https://doi.org/10.18720/MCE.87.1.

[20] Ahmadie Amiri H, Pournamazian Najafabadi E, Esmailpur Estekanchi H, Ozbakkaloglu T. Performance-based seismic design and assessment of low-rise steel special moment resisting frames with block slit dampers using endurance time method. Eng Struct 2020;224. https://doi.org/10.1016/j.engstruct.2020.110955.

[21] Kim J, Kim MC, Kim DK. Preliminary study on a composite steel slit damper. J Mech Sci Technol 2021. https://doi.org/10.1007/s12206-021-0806-7.

[22] Oh SH, Park HY. Experimental study on seismic performance of steel slit damper under additional tensile load. J Build Eng 2022;50. https://doi.org/10.1016/j.jobe.2022.104110.

[23] Lee KS, Lee BG, Jung JS. Seismic Strengthening of R/C Buildings Retrofitted by New Window-Type System Using Non-Buckling Slit Dampers Examined via Pseudo-Dynamic Testing and Nonlinear Dynamic Analysis. Appl Sci 2022;12. https://doi.org/10.3390/app12031220.

[24] Rousta AM, Shoja S, Safaei Ardakani MA. Investigating Cyclic and Pushover Performance of Different Metallic Yielding Dampers. J Rehabil Civ Eng 2023;11. https://doi.org/10.22075/JRCE.2022.26848.1639.

[25] ABAQUS computer software 2019.

[26] ATC. Guidelines for cyclic seismic testing of components of steel structures. vol. 24. 1992.

[27] Timoshenko S. Elementary theory and problems. Van Nostrand; 1940.

[28] Brancheriau L. Influence of cross section dimensions on Timoshenko's shear factor - Application to wooden beams in free-free flexural vibration. Ann For Sci 2006;63. https://doi.org/10.1051/forest:2006011.

[29] Chinwuba Ike C. Timoshenko Beam Theory for the Flexural Analysis of Moderately Thick Beams – Variational Formulation, and Closed Form Solution. Tec Ital J Eng Sci 2019;63. https://doi.org/10.18280/ti-ijes.630105.

[30] Gaur A, Dhurvey P. Comparative Study of Beam Theories on the Effect of Span-Depth Ratio for Symmetric and Un-symmetric Loadings. IOP Conf. Ser. Mater. Sci. Eng., vol. 936, 2020. https://doi.org/10.1088/1757-899X/936/1/012047.

[31] ASTM E2126. Standard Test Methods for Cyclic (Reversed) Load Test for Shear Resistance of Vertical Elements of the Lateral Force Resisting Systems for Buildings. ASTM Int 2019.